International Journal of Mass Spectrometry 281 (2009) 72–78

Contents lists available at ScienceDirect

International Journal of Mass Spectrometry

journal homepage: www.elsevier.com/locate/ijms

Formation, distribution, and structures of oxygen-rich iron and cobalt oxide clusters

Shi Yin [a,b], Wei Xue [a,b], Xun-Lei Ding [a], Wei-Gang Wang [a], Sheng-Gui He [a,*], Mao-Fa Ge [a,*]

[a] Beijing National Laboratory for Molecular Sciences (BNLMS), State Key Laboratory for Structural Chemistry of Unstable and Stable Species, Institute of Chemistry, Chinese Academy of Sciences, Beijing 100190, China
[b] Graduate University of the Chinese Academy of Sciences, Beijing 100039, China

ARTICLE INFO

Article history:
Received 13 October 2008
Received in revised form 11 December 2008
Accepted 11 December 2008
Available online 25 December 2008

Keywords:
Iron oxide clusters
Cobalt oxide clusters
Time of flight mass spectrometry
Density functional theory

ABSTRACT

A time of flight mass spectrometer coupled with a laser ablation/supersonic expansion cluster source is used to study the formation and distribution of cationic iron and cobalt oxide clusters. Although the distributions of iron oxide clusters ($Fe_mO_n^q$, $q=0, \pm1$) have been extensively reported in literature, new and very interesting distribution of $Fe_mO_n^+$ clusters is observed in this study. Under saturated O_2 growth conditions, the smallest (leading) cluster in $m=2k+1$ ($k=2-14$) cluster series is with stoichiometry of $Fe_{2k}O_{3k}FeO^+$, which is perfect (iron atoms are perfectly oxidized) in terms of average oxidation states of iron (Fe^{3+}) and oxygen (O^{2-}) atoms. For $m=2k$ ($k=2-15$) cluster series, the leading cluster is either $Fe_{2k}O_{3k}^+$ (the least over-oxidized) or $Fe_{2k}O_{3k-1}^+$ (the least under-oxidized). Density functional theory (DFT) calculations indicate that these leading clusters are with unexpected structures although their appearance in the mass spectra is predictable. These clusters may serve as good models for predicting or interpreting novel properties of Fe_2O_3 nano-materials. The distribution of the cobalt oxide clusters ($Co_mO_n^+$) under saturated O_2 growth conditions is complex and very different from that of $Fe_mO_n^+$. A very interesting result for cobalt species is that two clusters $Co_{11}O_{13}^+$ and $Co_{12}O_{13}^+$ are missing in the cluster distribution although their oxygen-neighbor clusters $Co_{11}O_{12,14}^+$ and $Co_{12}O_{12,14}^+$ are generated. This suggests relatively high stability for $Co_{11}O_{12}^+$ and $Co_{12}O_{12}^+$ clusters. The DFT calculations predict that $Co_{12}O_{12}$ cluster are with tower or cage structure rather than the compact NaCl-like arrangement that is found for bulk CoO.

1. Introduction

Cluster formation and growth can offer insight into the transition from molecular behavior to condensed phase behavior [1–6]. In addition, bonding properties of clusters are sometimes completely different from those of the corresponding bulk materials, leading to a possibility to synthesize entirely novel materials [6]. Iron and cobalt oxides are very important materials that can be used as catalysts, semi-conductors, insulators, data storage media, etc. MO and M_3O_4 (M = Fe, Co) and Fe_2O_3 are normal and stable compositions of iron and cobalt oxides. The formation and property studies of iron and cobalt oxide clusters have been extensively reported by several research groups [7–24]. A careful literature survey indicates that most of the studied clusters ($Fe_mO_n^q$ and $Co_mO_n^q$, $q=0, \pm1$) are oxygen-poor ($n/m<1$) [14-18] or oxygen-near-equivalent ($n/m\approx1$) [7–9,19,20,24]. The oxygen-rich clusters with $n/m\approx3/2$ and 4/3 that correspond respectively to bulk materials of Fe_2O_3 and Co_3O_4 (Fe and Co are in the highest normal oxidation states) have not been systematically studied. The investigations of these oxygen-rich clusters are only reported for small clusters ($m\leq5$). We attempt to generate and study the distributions of large oxygen-rich iron and cobalt oxide clusters in this work. Since Fe_2O_3 and Co_3O_4 nano-materials are efficient catalysts for reactions such as low-temperature CO oxidation [25–29], it may be possible to interpret the mechanistic details in these catalytic processes based on the bonding and reactivity properties of Fe_mO_n ($n/m\approx3/2$) and Co_mO_n ($n/m\approx4/3$) clusters.

For early transition metals, generations of gas phase clusters series Ti_mO_n ($n/m\approx2$) [30,31], V_mO_n ($n/m\approx5/2$) [32,33], Cr_mO_n ($n/m\approx3$) [34,35], and $(WO_3)_n^-$ ($n=1-3$) [36–38] have been reported. These clusters correspond to their bulk oxides with metals being in the highest normal oxidation states. For late transition metals such as iron, generation of large Fe_mO_n clusters with $n/m\approx3/2$ is not obvious from available literature reports. Shin et al. [19,20] studied the distribution of neutral iron oxide cluster with single photon ionization at 118 nm and multi-photon ionization at 193 nm. They suggested that the thermodynamically stable neutral clusters are

* Corresponding authors. Tel.: +86 10 62536990; fax: +86 10 62559373.
E-mail addresses: shengguihe@iccas.ac.cn (S.-G. He), gemaofa@iccas.ac.cn (M.-F. Ge).

1387-3806/$ – see front matter © 2008 Elsevier B.V. All rights reserved.
doi:10.1016/j.ijms.2008.12.014

$Fe_mO_{n=m+0-2}$ ($n/m \approx 1$ for large m) under saturated O_2 growth conditions. In the above mentioned investigations, the method of laser ablation was generally used to generate the metal oxide clusters. It should be pointed out that an alternative approach to generate metal oxide clusters is via electrospray ionization [39,40]. With density functional theory (DFT) calculations, Jones et al. predicted that $Fe_mO_{n=m+0-2}$ clusters with structures of rings, towers, hollow drums, or cages are quite stable [41,42]. Very recently, Molek et al. studied the photo-dissociation of cationic iron oxide clusters [24]. They concluded that clusters $Fe_mO_n^+$ with $m = n$ have the greatest stability. These studies imply that the generation of large $Fe_mO_n^q$ clusters with (or purely with) $n/m \approx 3/2$ may be difficult.

Cobalt and iron are neighbors in the periodic table. Both of them are with +2 and +3 as normal oxidation states. The available literature reports indicate that there are strong similarities between (distributions of) $Fe_mO_n^q$ and $Co_mO_n^q$ clusters with $n/m < 1$ or $n/m \approx 1$. Sakurai and co-workers [14–18] studied formation and distribution of oxygen-deficient iron and cobalt oxide clusters. Clusters with the form of $M_mO_{(m+3)/2}$ (M = Fe and Co; $m = 3, 5, 7, .$) are relatively stable. Both $Fe_mO_{n/m\approx1}$ and $Co_mO_{n/m\approx1}$ (for large m) are generated after reactions of preformed iron [7–9] and cobalt [43] clusters with O_2. It is interesting to study whether the distributions of oxygen-rich iron and cobalt oxide clusters are similar in the case that these clusters can be generated.

In this work, a time of flight mass spectrometer (TOF-MS) coupled with a laser ablation/supersonic expansion cluster source is used to study the formation and distribution of $Fe_mO_n^+$ and $Co_mO_n^+$ clusters under saturated O_2 growth conditions. Very interesting cluster distributions unreported in literature are observed. The DFT calculations are performed to predict the structures of some typical clusters.

2. Method

The experiments performed in this work are conducted with a TOF-MS coupled with a laser ablation/supersonic expansion cluster source and a fast flow reactor [44]. The design of the apparatus is similar to the one used in ref. [45]. The vacuum system of the apparatus consists of two chambers. One of the chambers is used for cluster generation/reaction and the other is for cluster ion detection. The two chambers are connected through a 5 mm diameter skimmer. The metal (iron or cobalt) oxide clusters are generated by the reaction of laser ablation generated metal plasmas with O_2 seeded in the helium (99.999% purity) carrier gas. The typical backing pressure of the He gas is 5 atm. To generate the metal plasmas, a Nd:YAG laser beam (532 nm, 5 mJ/pulse, 8 ns duration, 10 Hz) is focused onto an iron or cobalt metal disk (16 mm diameter, 0.13 mm thickness, 99.7% purity from Aldrich). The disk is rotated and translated to continually expose a fresh surface. The carrier gas seeded with different concentrations of O_2 is controlled by a pulsed valve (General Valve, series 9). The clusters are formed in a narrow cluster formation channel (2 mm inner diameter – I.D.) that contains a relaxation zone (3 mm I.D.). The lengths of the channel and the relaxation zone are adjustable to optimize the cluster growth conditions. The typical lengths used are 1 cm for the relaxation zone and 2 cm for the rest of the channel. A fast flow reactor with 6 mm I.D. and 8 cm length is coupled with the narrow cluster formation channel. The generated cationic clusters can exit the empty tube reactor and pass through the 5 mm skimmer for detection through TOF-MS. Before the detection, the clusters can also react in the tube reactor with reactants (C_xH_y, CO, N_2, etc.) diluted in helium/argon carrier gas that is controlled by a second pulsed valve. The cluster ions are extracted, accelerated, and focused by a set of ion optics. The synchronization of laser firing, pulsed valve opening(s), and ion detection is managed through commercial available and home made electronics. The mass signal is generated by a dual micro-channel plate detector and recorded with a digital acquisition card that is controlled by a Labview based program. Mass resolution ($M/\Delta M$) of 300 can be obtained. In this study, we focused on the formation, distribution, and structures of oxygen-rich iron and cobalt oxide clusters. The cluster reactivity toward several gas molecules studied by using the fast flow reactor will be presented in future.

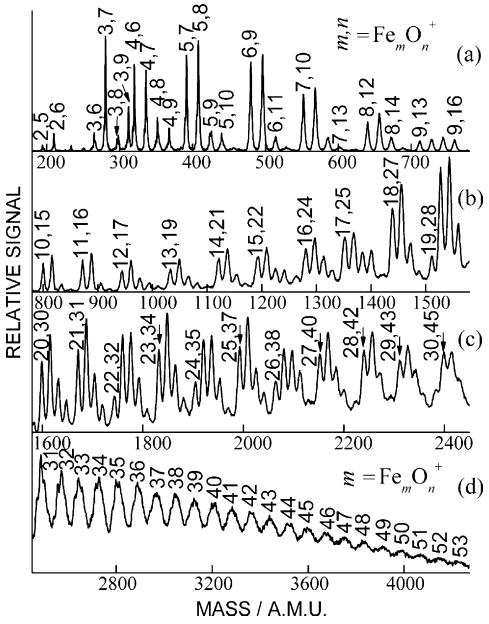

Fig. 1. The TOF mass spectra for distribution of iron oxide clusters generated under 10% O_2 concentration. The $Fe_mO_n^+$ clusters are denoted as m, n and m in the figure for cluster masses below and above 2500 amu, respectively.

The DFT calculations are performed to predict the structures of $(Fe_2O_3)_m$ with $m = 2–6$ and $(CoO)_m$ with $m = 2–4$, 6, 9, and 12. The hybrid B3LYP exchange-correlation functional [46–48] is adopted. The Los Alamos effective core potential plus valence double-zeta basis set [49–51] is used on Fe and Co atoms while the Dunning/Huzinaga valence double-zeta basis set (D95V) [52] is used on O atom. The basis sets are denoted as LanL2DZ in Gaussian 03 program [53] that is used for all the calculations. The energies reported in this study are zero-point vibration corrected energies.

3. Results

3.1. Distribution of iron oxide clusters

The TOF mass spectra of $Fe_mO_n^+$ ($m = 2–53$) clusters generated under 10% O_2 condition are plotted in Fig. 1. The mass spectra generated under different concentrations of O_2 are given in Fig. S1 (see Supplementary Information). Small clusters including Fe^+ can be generated when low concentration of O_2 is used (Fig. S1a). This provides us an opportunity to determine the absolute mass of the generated clusters shown in Fig. 1a with 2–5 iron atoms (see Supplementary Information, Table S1–S7). Fig. 2 plots the mass spectra in the range of 50–350 amu where hydrogen impurity peaks can be resolved. The hydrogen impurity peaks can be assigned as iron oxide clusters with one or more H_2O molecules: $Fe_mO_n(H_2O)_x^+$. The signals of the hydrogen containing peaks (m, n, $x = 1$, 2, 1–3; m, n, $x = 2$, 2–4, 1; m, n, $x = 2$, 2, 2 and 3, 4, 1) are relatively strong if the gas-handling systems are not carefully pumped (Fig. 2a). In contrast, these impurity peaks become relatively weak if the gas-handling systems are carefully pumped (Fig. 2b).

We have also tried to put a liquid nitrogen cooled molecular sieve in between the pulsed valve (a 1 m long copper tube in

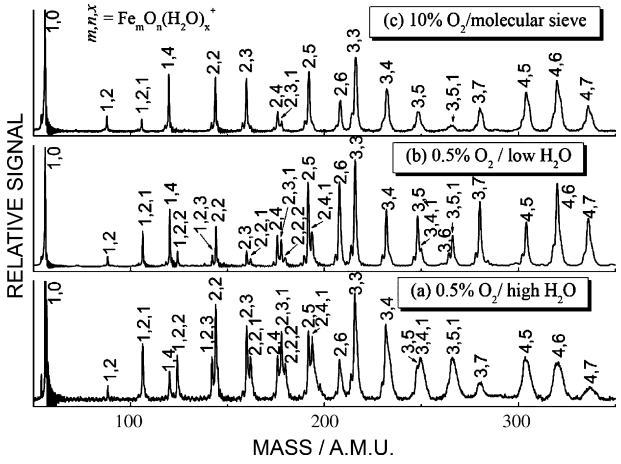

Fig. 2. The TOF mass spectra of small iron oxide clusters generated under three different experimental conditions: (a) 0.5% O_2 prepared with and delivered through not carefully pumped gas-handling systems; (b) 0.5% O_2 prepared with and delivered through carefully pumped gas-handling systems [replot of Fig. S1a in the range of 50–350 amu]; and (c) 10% O_2 prepared with and delivered through carefully pumped gas-handling systems and a liquid nitrogen cooled molecular sieve between the pulsed valve and the gas bomb is used. The $Fe_mO_n^+$ and $Fe_mO_n(H_2O)_x^+$ clusters are denoted as m, n and m, n, x, respectively.

air connects the pulsed valve and the molecular sieve) and the gas bomb that contains the high pressure He seeded with 10% O_2. The mass spectrum such obtained is given in Fig. 2c. This method further decreases the relative signal magnitudes of the hydrogen impurity peaks, for example, peaks of $FeO_2(H_2O)_{2-3}^+$, $Fe_2O_2(H_2O)_{1-2}^+$, and $Fe_2O_4H_2O^+$ disappear almost completely. This experiment also verifies that the assignments of the peaks to pure $Fe_mO_n^+$ in Fig. 2b are correct since relative magnitudes of $Fe_mO_n^+$ peaks do not decrease upon using the molecular sieve. We note that the low-temperature molecular sieve may also trap O_2 significantly, so the true concentration of O_2 after the molecular sieve is lower than as prepared (10% in the gas bomb). As a result, the distribution of $Fe_mO_n^+$ clusters in Fig. 2c is similar to that of the clusters generated under 0.5% O_2 condition without using the molecular sieve (Fig. 2b). The experimental setup using the low-temperature molecular sieve is relatively complicated and the true concentration of O_2 in this case is unknown, so we just use the carefully pumped gas-handling systems without the molecular sieve to generate the mass distributions in Figs. 1, S1, and 3 (see below).

As can be seen in Fig. 2b, although there are some hydrogen impurity peaks, the main part of the mass distribution is due to pure iron oxide clusters. In addition, the sufficient mass resolution for $Fe_{2-5}O_n^+$ clusters tells that almost all of the small clusters in Fig. 1 do not contain any hydrogen atoms: among the 14 marked $Fe_{2-5}O_n^+$ mass peaks in Fig. 1a, only two weak peaks ($Fe_3O_8^+$ and $Fe_5O_9^+$) have high-mass shoulders due to hydrogen impurities. We thus assign the observed mass peaks in Fig. 1 to pure $Fe_mO_n^+$ clusters (see Supplementary Information, Table S5–S16 for details of the assignments). Iron has four stable natural isotopes and their abundances are as follows: ^{54}Fe/5.845%, ^{56}Fe/91.754%, ^{57}Fe/2.119%, and ^{58}Fe/0.282% [54]. A simulation of the isotopomer distribution for $Fe_2O_5^+$, $Fe_4O_6^+$, $Fe_{10}O_{15}^+$, and $Fe_{20}O_{30}^+$ clusters is given in Fig. S2 (see Supplementary Information). This simulation tells that the side or shoulder peaks on the low-mass side of the main peaks presented in Fig. 1a ($Fe_4O_6^+$, $Fe_5O_7^+$, $Fe_6O_9^+$, etc.) and Fig. 2b ($Fe_2O_5^+$, $Fe_3O_3^+$, $Fe_4O_5^+$, etc.) are due to ^{54}Fe isotopomers.

Fig. 1c shows that the TOF-MS can resolve one oxygen atom up to about 2400 amu. The clusters with fixed number (m) of iron (or cobalt, Fig. 3) atoms and different number of oxygen atoms are denoted as Fe_m (or Co_m) cluster series in this study. Fig. 1 shows that each Fe_m cluster series consists of 3–4 clusters. For instance, Fe_4 series consists of $Fe_4O_6^+$, $Fe_4O_7^+$, $Fe_4O_8^+$, and $Fe_4O_9^+$ clusters. The smallest (leading) clusters in $Fe_{m\geq4}$ series are $Fe_4O_6^+$, $Fe_5O_7^+$, $Fe_6O_9^+$, $Fe_7O_{10}^+$, $Fe_8O_{12}^+$, $Fe_9O_{13}^+$, $Fe_{10}O_{15}^+$, etc. The distribution of these leading clusters is very interesting and well predictable. For Fe_m series with odd ($m = 2k + 1$) number of iron atoms, the leading clusters are with stoichiometry of $Fe_{2k}O_{3k}FeO^+$ for $k = 2$–14 (without exception!). Iron atom in FeO^+ diatomic molecule can be considered in +3 oxidation state. $(Fe_2O_3)_kFeO^+$ clusters are thus perfect in terms of average oxidation states of iron (Fe^{3+}) and oxygen (O^{2-}) atoms, i.e., iron atoms are perfectly oxidized to +3 valence state in these clusters. For Fe_m series with even ($m = 2k$) number of iron atoms, the leading clusters are with stoichiometry of $Fe_{2k}O_{3k}^+$ for $k = 2$–5, 7–10, and 14–15 or $Fe_{2k}O_{3k-1}^+$ for the rest of k values in the range of 2–15. $Fe_{2k}O_n^+$ clusters cannot be perfect in terms of the average oxidation states of iron and oxygen atoms, but iron atoms in $Fe_{2k}O_{3k}^+$ and $Fe_{2k}O_{3k-1}^+$ clusters are (averagely) the least over-oxidized and the least under-oxidized, respectively.

The 10% O_2 can be considered as saturated O_2 growth conditions in this study because very similar cluster distribution as in Fig. 1 can be generated when higher concentration (such as 20%) of O_2 is used. The clusters shown in Fig. 1 are all oxygen-rich ($n/m > 1.5$ or $\approx$1.5). Oxygen-near-equivalent ($n/m \approx 1$) or oxygen-poor ($n/m < 1$) clusters can be eventually generated when very low concentration (<0.5%) of O_2 is used (see Supplementary Information, Fig. S1).

3.2. Distribution of cobalt oxide clusters

The TOF mass spectra of $Co_mO_n^+$ clusters generated under saturated (10%) O_2 growth conditions are plotted in Fig. 3. Although some of the $Co_{2-4}O_n^+$ peaks ($Co_2O_5^+$, $Co_3O_{4,5}^+$, $Co_4O_{5,6}^+$) have high-mass shoulders due to hydrogen impurities, all of the leading clusters ($Co_3O_3^+$, $Co_4O_4^+$, $Co_5O_6^+$, etc.) in Co_{3-14} cluster series are with narrow and symmetric mass peaks (note that cobalt has a single natural isotope). These leading clusters can be assigned as pure $Co_mO_n^+$ clusters. There may be hydrogen impurities in the peaks of other (non-leading) clusters (such as $Co_6O_9^+$ and $Co_7O_{10}^+$ with relatively broad mass peaks), but one can consider that the main contribution to the mass peaks is still from the pure $Co_mO_n^+$ clusters.

Unlike iron oxide clusters, of which the leading clusters of $Fe_{m\geq4}$ series are with well defined stoichiometry (Fig. 1 and Section 3.1), the distribution of $Co_mO_n^+$ clusters (Fig. 3) are complex. There are

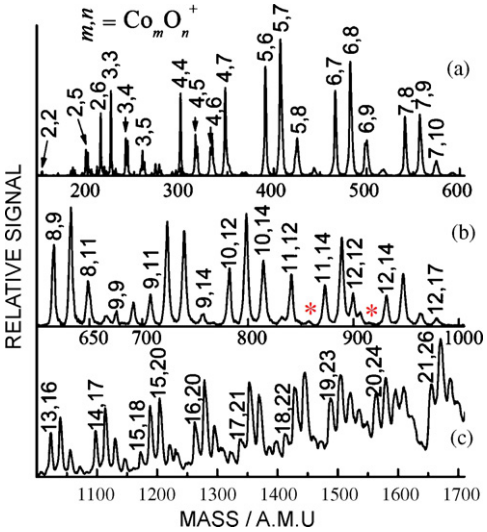

Fig. 3. The TOF mass spectra for distribution of cobalt oxide clusters generated under 10% O_2 concentration. The $Co_mO_n^+$ clusters are denoted as m, n in the figure. Two asterisks in panel (b) indicate the peak positions of $Co_{11}O_{13}^+$ and $Co_{12}O_{13}^+$ clusters.

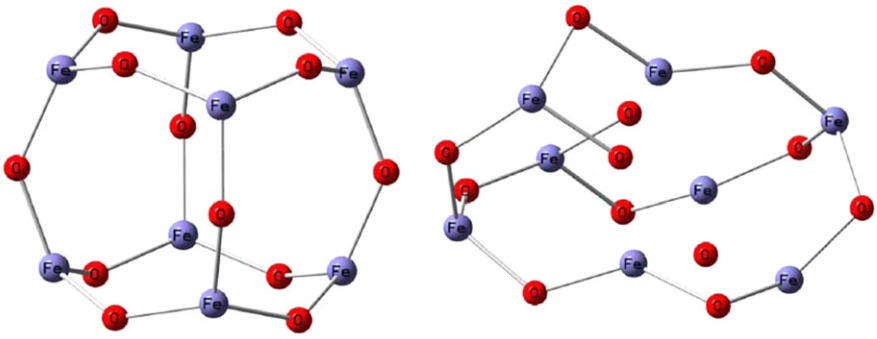

Fig. 4. The DFT optimized structures and relative energies of the Fe_8O_{12} cluster with O_h (a) and C_1 (b) symmetries.

fewer oxygen atoms in the leading clusters of Co_m series than in those of Fe_m, for instance, $Co_4O_4^+$ versus $Fe_4O_6^+$, $Co_5O_6^+$ versus $Fe_5O_7^+$, $Co_6O_7^+$ versus $Fe_6O_9^+$, etc. Most of the leading clusters ($Co_mO_n^+$) in $Co_{m>4}$ series are with $n>m$. The two exceptions are $Co_9O_9^+$ and $Co_{12}O_{12}^+$. An interesting result shown in Fig. 3 is that $Co_{11}O_{13}^+$ and $Co_{12}O_{13}^+$ are missing (or barely observed) in Co_{11} and Co_{12} series, respectively. Their oxygen-neighbor clusters $Co_{11}O_{12,14}^+$ and $Co_{12}O_{12,14}^+$ are apparently generated.

3.3. Computational results

The very interesting leading cluster distribution of Fe_m series [especially for $m=2k+1$ series: $(^{III}Fe_2^{II}O_3)_k(^{III}Fe^{II}O)^+$] hints that the structures and/or energetics of neutral $(Fe_2O_3)_k$ clusters may be special. A systematic DFT study on $(Fe_2O_3)_{2-6}$ clusters has been performed. The reason to perform theoretical calculations on neutral clusters $(Fe_2O_3)_k$ instead of the experimentally observed cationic clusters $(Fe_2O_3)_kFeO^+$ [note that $(Fe_2O_3)_k^+$ is not perfect in terms of iron and oxygen valence state] is that the structures of $(Fe_2O_3)_n$ clusters may be with high symmetries (see below). It is interesting to study if the highly symmetric structures are stable or not. Moreover, the stability analysis of $M_mO_n^+$ ($M_mO_n^+ \rightarrow M_xO_y^+ + M_{m-x}O_{n-y}$) involves both neutral and cationic clusters, which costs additional computational resources. It is expected that the general bonding properties of $M_mO_n^+$ are similar to those of M_mO_n especially for large clusters. It should be pointed out that iron and cobalt oxide cluster systems are challenging for state-of-the-art quantum chemistry calculations. One should keep in mind that the connections between theory and experiment in this study are tentative.

The detailed description of the theoretical results for $(Fe_2O_3)_{2-6}$ clusters is not the subject of this work and it can be found in a separate publication [55]. Two typical optimized structures and relative energies of Fe_8O_{12} cluster are given in Fig. 4 as an example. The cage structures [such as Fig. 4a] of $(Fe_2O_3)_{2-6}$ cluster are with all positive vibrational frequencies. However, non-cage structures [such as Fig. 4b] of $(Fe_2O_3)_{3-6}$ clusters are more stable than the cage structures. These non-cage structures are unexpected and unpredictable, in contrary to the well predictable leading cluster distribution in Fig. 1.

The optimized structures of Co_mO_m clusters are given in Fig. 5. The Co_2O_2 and Co_3O_3 clusters have four-membered and six-membered ring structures, respectively. The compact cubic structure (4b) of Co_4O_4 is less stable than the ring structure (4a) by 0.66 eV. The structure of Co_6O_6 with compact cubic subunits (6b) is higher in energy by 0.46 eV than the tower structure (6a) composed of two Co_3O_3 rings. Similar results are found for Co_9O_9 and $Co_{12}O_{12}$ clusters: the Co_3O_3 based tower structures (9a and 12a) are more stable than the cubic based structures (9c and 12c) by 0.96 and 1.22 eV for Co_9O_9 and $Co_{12}O_{12}$, respectively. For $Co_{12}O_{12}$, the Co_4O_4 based structures (12d) are less stable than the 12a structure by 1.46 eV. The cage type structures of Co_9O_9 (9b) and $Co_{12}O_{12}$ (12b) are slightly higher in energies than the tower structures (9a and 12a). Although it is hard to make a very accurate theoretical prediction for transition metal systems (cobalt oxides in this study), it may be safe to conclude qualitatively that ring, tower, or cage structure of Co_mO_m ($m=3, 4, 6, 9, 12$) is more stable than the compact cubic based structures.

4. Discussion

4.1. Comparison with previous results

The iron oxide clusters generated under saturated O_2 growth conditions are all oxygen-rich and the oxygen to iron ratio is close to 1.5 for large clusters (Fig. 1). This cluster distribution is different from what have been reported in literature, where oxygen-deficient or oxygen-near-equivalent clusters ($Fe_mO_n^q$, $n/m<1$ [14–18] or $n/m\approx1$ [19,20,24] for large m) are generated. The method (laser ablation/supersonic expansion) used in this study to generate the clusters is very similar to the one adopted by Shin et al. [19,20] on neutral Fe_mO_n and by Molek et al. [24] on cationic $Fe_mO_n^+$. Oxygen-near-equivalent clusters (such as $Fe_4O_4^+$, $Fe_4O_5^+$, $Fe_5O_6^+$, see Fig. 1 of Ref. [24]) are still present under 20% O_2 condition in the work carried out by Molek et al. while these clusters disappear completely under 10% O_2 condition in our experiment. These clusters (such as $Fe_4O_5^+$) can be observed in our experiment when very low concentration (<0.5%) of O_2 is used. The discrepancy of the cluster distribution is possibly due to use of particular design of the cluster formation channel with a relaxation zone in our experiment.

The length (L_1) of the relaxation zone and the length (L_2) of the channel after the relaxation zone (L_1) are adjustable in our experiment. L_1 and L_2 are set to 10 mm and 20 mm, respectively, in generating the cluster distribution in Fig. 1. It has been tested that when shorter values of L_1 and L_2 (such as $L_1=2$ mm and $L_2=10$ mm) are used, $Fe_mO_n^+$ clusters with $n/m\approx1$ can be observed under 10% O_2 conditions. The number of collisions between iron plasma (or initially formed small iron oxide clusters) and O_2 is increased if longer values of L_1 and L_2 are used, which increases the *effective* concentration of O_2 in the carrier gas. Moreover, increased number of collisions results in more energy dissipation from the plasma to the (helium) carrier gas, which leads to lower *effective* temperature at which the clusters are formed. Our DFT calculations [55] on the energetics of Fe_4O_{0-8} clusters indicates that oxidation of Fe_4O_4 and Fe_4O_5 ($Fe_4O_n + O_2/2 \rightarrow Fe_4O_{n+1}$ and $Fe_4O_n + O_2 \rightarrow Fe_4O_{n+2}$ for $n=4$ and 5) clusters are thermodynamically not favorable ($\Delta G>0$) at

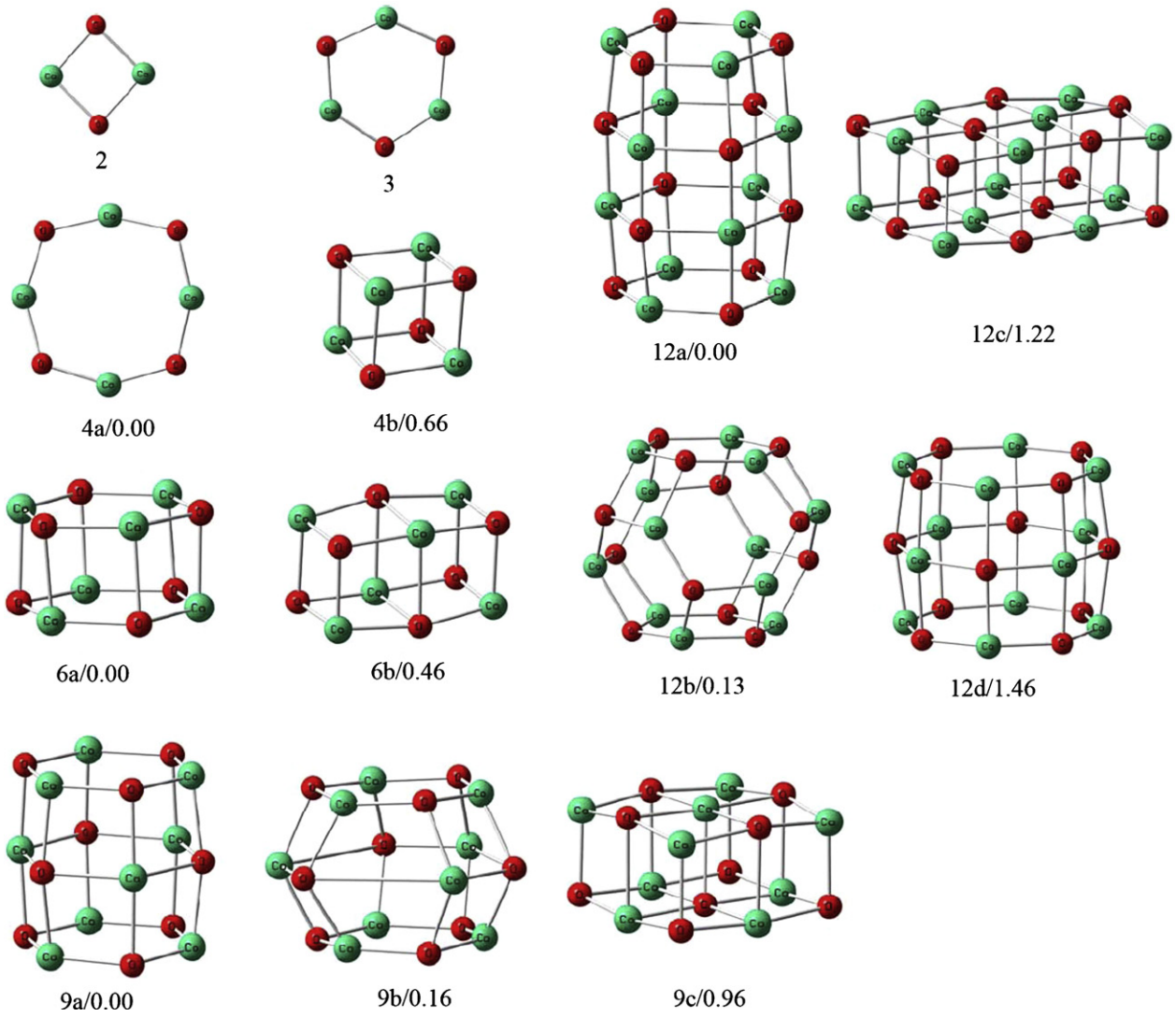

Fig. 5. The DFT optimized structures and relative energies of the Co_mO_m (m = 2–4, 6, 9, and 12) clusters. The structure isomers (x = a, b, etc.) and relative energies (E in eV, zero-point vibration corrected) are given as mx/E for Co_mO_m clusters. The structures are with C_1 symmetry except 2 (C_{2v} $^7B_2$), 9a (C_s, $^{25}A''$), and 12d (D_{4h}, $^{37}B_{1g}$).

1000 K and favorable ($\Delta G < 0$) at 298 K. Although the calculations are carried out on neutral clusters, it may be used to predict that the observation of $Fe_4O_4^+$ and $Fe_4O_5^+$ cluster cations under saturated O_2 growth conditions depends on the temperature at which the clusters are formed. It should be pointed out that the detailed mechanisms of cluster formation under laser ablation conditions are very complex. In addition, there is possibility that the cluster source with O_2 in the bath gas may lead to isomeric oxygen complexes as suggested for mono iron, chromium, and rhenium species [56–58] and shown for $V_mO_n^+$ [59,60] and $Fe_2O_2^+$ [61,62] clusters. Our discussion that the iron oxide cluster distribution may be understood based on the specific energetics of the most stable cluster isomers under different temperatures just provides one simple idea for a complex problem.

It is not a surprise that different cluster distributions can be generated under different conditions. However, it is surprising to find that the leading cluster distribution ($Fe_{2k}O_{3k}FeO^+$ for k = 2–14) is perfect in terms of average oxidation states of iron (Fe^{3+}) and oxygen (O^{2-}) atoms, under saturated O_2 growth conditions. This means that $Fe_{2k}O_{3k}FeO^+$ (or neutral $Fe_{2k}O_{3k}$) clusters are with special structures and/or energetics. Our DFT calculations [55] have indicated that the ground states of $Fe_{2k}O_{3k}$ (k = 3–6) are not with special structures such as the cages of $(V_2O_5)_k$ clusters (without the terminal V=O bonds) [63]. On the contrary, some unexpected structures are found to be more stable than the cages. Meanwhile, the DFT calculations predict that the oxidation of Fe_4O_6 cluster by O_2 ($Fe_4O_6 + O_2/2 \rightarrow Fe_4O_7$ and $Fe_4O_6 + O_2 \rightarrow Fe_4O_8$) is thermodynamically not favorable at room temperature or high [55]. This provides an idea that $Fe_{2k}O_{3k}FeO^+$ is possibly with specific thermodynamics although we cannot exclude the possibility that special kinetics in the cluster formation processes can determine the final cluster distribution. An interesting fact may be that the mass spectra in Fig. 1 are purely dictated by valence electron counting: Fe^{3+} and O^{2-}. The bonding properties of $Fe_{2k}O_{3k}$ clusters are different from those of bulk Fe_2O_3 [55]. The successful generation of $Fe_mO_n^+$ clusters with $n/m \approx 3/2$ provides a possibility to interpret or predict novel properties of Fe_2O_3 nano-particles by using $Fe_mO_n^+$ as models.

The cobalt oxide distribution in Fig. 3 is more or less similar to what have been reported in literature, where oxygen-near-equivalent clusters ($Co_mO_n^{\pm 1}$, $n/m \approx 1$) are generated. [43,64] The $Co_mO_n^+$ clusters with $n/m \approx 1$ are also generated in this study. The difference is that the clusters with more oxygen atoms are also produced. The clusters generated previously can be understood as $Co_mO_m^+$ or $Co_mO_{m+1}^-$ clusters containing zero to one more cobalt atom, while they are $Co_mO_m^+$ clusters containing zero to more Co_2O_3 moieties in this study.

4.2. Comparison between iron and cobalt species

Under saturated O_2 growth conditions, the distribution of cobalt oxide clusters is very different from that of iron oxide clusters although iron ($3d^6 4s^2$) and cobalt ($3d^7 4s^2$) are neighbors in periodic table. The difference is however, not a surprise if one considers the fact that the bulk Fe_2O_3 is common and stable form of iron oxides while Co_2O_3 is usually stable as the hydrated compound [65] or as Co_3O_4 (=$CoOCo_2O_3$). The cobalt oxide clusters generated under saturated O_2 growth conditions are generally with distribution of $(CoO)_m(Co_2O_3)_n^+$, for which the average oxidation state of cobalt is less than 3. In contrast, average oxidation state of iron in the clusters $[(Fe_2O_3)_n(FeO)_{0,1}O_{0-3}^+]$ is equal to or higher than 3. This supports and is supported by the conclusion that iron is significantly more reactive than cobalt toward O_2 oxidation.

4.3. Special distribution of cobalt oxide clusters

In Fig. 5, the Co_3O_3 ring based tower structures of Co_6O_6, Co_9O_9, and $Co_{12}O_{12}$ are more stable than the corresponding compact NaCl-like cubic structures. This is interesting considering that the bulk CoO crystal is with the NaCl-like lattice. In Fig. 3, from $m = 5$, the leading clusters (i.e., $Co_5O_6^+$, $Co_6O_7^+$, $Co_7O_8^+$, $Co_8O_9^+$, $Co_{10}O_{12}^+$, $Co_{11}O_{12}^+$, $Co_{13}O_{16}^+$, etc.) in Co_m cluster series generally have fewer cobalt atoms than the oxygen atoms. The only two exceptions are $Co_9O_9^+$ and $Co_{12}O_{12}^+$. The experiment thus suggests relatively high geometry stability (versus composition stability) [66] for $Co_9O_9^+$ and $Co_{12}O_{12}^+$ clusters, which is probably related with the tower (9a, 12a) or the cage (9b, 12b) structures of Co_9O_9 and $Co_{12}O_{12}$. It is noticeable that the cage structures of Zn_9O_9 and $Zn_{12}O_{12}$ similar as 9b of Co_9O_9 and 12b of $Co_{12}O_{12}$ (Fig. 5) has been predicted to be relatively stable among $(ZnO)_{m=2-18}$ clusters [67].

It is interesting to explain the result that two cobalt oxide clusters ($Co_{11}O_{13}^+$ and $Co_{12}O_{13}^+$) are missing in Fig. 5. The high geometry stability of $Co_{12}O_{12}^+$ cluster mentioned above may well be used to explain the fact that $Co_{12}O_{13}^+$ is missing under saturated O_2 growth conditions. Considering that the Co_{10} cluster series starts with $Co_{10}O_{12}^+$, the Co_{12} series "should" start with $Co_{12}O_{14}^+$. However, the $Co_{12}O_{12}^+$ cluster is relatively stable, which causes an *abnormal* distribution of the Co_{12} cluster series ($Co_{12}O_{13}^+$ is missing). The same logic can be used to explain the missing of $Co_{11}O_{13}^+$ cluster, which suggests that the $Co_{11}O_{12}^+$ cluster is with relatively high geometry stability. To conclude, there are strong evidences from the experiments that the $Co_9O_9^+$, $Co_{11}O_{12}^+$, and $Co_{12}O_{12}^+$ clusters are relatively stable. It should be pointed out that the high affinity of an O_2 ligand to $Co_{11,12}O_{13}^+$ (to form $Co_{11,12}O_{15}^+$) may also be a reason that $Co_{11,12}O_{13}^+$ are missing under the saturated O_2 growth conditions. The results in this study invite further experimental works such as reactivity and stability (photodissociation, collision induced dissociation) investigations on these clusters.

5. Conclusions

A TOF-MS coupled with a laser ablation cluster source has been employed to study the formation and distribution of cationic iron and cobalt oxide clusters under saturated O_2 growth conditions. Oxygen-rich $Fe_mO_n^+$ clusters with $n/m \approx 3/2$ for large m can be generated. Each Fe_m cluster series consists of 3–4 clusters with fix number (m) of iron and different number of oxygen atoms. The smallest (leading) clusters of Fe_m series are with stoichiometry of $Fe_{2k}O_{3k}FeO^+$ for $m = 2k + 1$ ($k = 2$–14) and $Fe_{2k}O_{3k}^+$ or $Fe_{2k}O_{3k-1}^+$ for $m = 2k$ ($k = 2$–15). These leading clusters are perfect ($Fe_{2k}O_{3k}FeO^+$) or nearly-perfect ($Fe_{2k}O_{3k}^+$ and $Fe_{2k}O_{3k-1}^+$) in terms of average oxidation states of iron (Fe^{3+}) and oxygen (O^{2-}) atoms. DFT calculations suggest that these leading clusters are with unexpected structures. These leading clusters may serve as good models for predicting or interpreting novel properties of Fe_2O_3 nano-materials. The cobalt is generally less reactive than iron toward O_2. The average oxidation states of cobalt in $Co_mO_n^+$ clusters generated under saturated O_2 growth conditions are between +2 and +3. Strong experimental evidences suggest that $Co_9O_9^+$, $Co_{11}O_{12}^+$, and $Co_{12}O_{12}^+$ are with relatively high stability. The tower or cage structures of Co_9O_9 and $Co_{12}O_{12}$ are more stable than the NaCl-like cubic structure that is found for bulk CoO. These clusters are possible building blocks for novel materials.

Acknowledgments

This work was supported by the Chinese Academy of Sciences (Hundred Talents Fund), the National Natural Science Foundation of China (Nos. 20703048 and 20673123), the 973 Programs (Nos. 2006CB932100, 2006CB806200, and 2006CB403701) of Ministry of Science and Technology of China.

Appendix A. Supplementary data

Supplementary data associated with this article can be found, in the online version, at doi:10.1016/j.ijms.2008.12.014.

References

[1] E.L. Mutterties, T.N. Rodin, E. Brand, C.F. Brucker, W. Pretzer, Chem. Rev. 79 (1979) 91.
[2] K. Eller, H. Schwarz, Chem. Rev. 91 (1991) 1121, and references therein.
[3] D. Schröder, H. Schwarz, Angew. Chem. Int. Ed. Engl. 34 (1995) 1973.
[4] G. Ertl, H.J. Freund, Phys. Today 52 (1999) 32.
[5] P.A. Hackett, S.A. Mitchell, D.M. Rayner, B. Simard, in: R. Russo, D.R. Salahub (Eds.), Metal-Ligand Interactions, Kluwer, Amsterdam, 1996, p. 289.
[6] Quantum Phenomena in Clusters and Nanostructures, in: S.N. Khanna, A.W. Castleman Jr. (Eds.), Springer, New York, 2003.
[7] S.J. Riley, E.K. Parks, G.C. Nieman, L.G. Pobo, S.J. Wexler, Chem. Phys. 80 (1984) 1360.
[8] G.C. Nieman, E.K. Parks, S.C. Richtsmeier, K. Liu, L.G. Pobo, S.J. Riley, High. Temp. Sci. 22 (1986) 115.
[9] S.J. Riley, in: D.R. Salahub, N. Russo (Eds.), Metal-Ligand Interactions: From Atoms, to Clusters to Surfaces, Kluwer Academic, The Netherlands, 1992, p. 17.
[10] L.S. Wang, H. Wu, S.R. Desai, Phys. Rev. Lett. 76 (1996) 4853.
[11] H. Wu, S.R. Desai, L.S. Wang, J. Am. Chem. Soc. 118 (1996) 5296.
[12] L.S. Wang, J. Fan, L. Lou, Surf. Rev. Lett. 3 (1996) 695.
[13] D. Schröder, P. Jackson, H. Schwarz, Eur. J. Inorg. Chem. (2000) 1171.
[14] M. Sakurai, K. Sumiyama, Q. Sun, Y. Kawazoe, J. Phys. Soc. Jpn. 68 (1999) 3497.
[15] M. Sakurai, K. Watanabe, K. Sumiyama, K. Suzuki, J. Phys. Soc. Jpn. 67 (1998) 2571.
[16] Q. Wang, Q. Sun, M. Sakurai, J.Z. Yu, B.L. Gu, K. Sumiyama, Y. Kawazoe, Phys. Rev. B 59 (1999) 12672.
[17] Q. Sun, M. Sakurai, Q. Wang, J.Z. Yu, G.H. Wang, K. Sumiyama, Y. Kawazoe, Phys. Rev. B 62 (2000) 8500.
[18] M. Sakurai, K. Watanabe, K. Sumiyama, K. Suzuki, J. Chem. Phys. 111 (1999) 235.
[19] D.N. Shin, Y. Matsuda, E.R. Bernstein, J. Chem. Phys. 120 (2004) 4150.
[20] D.N. Shin, Y. Matsuda, E.R. Bernstein, J. Chem. Phys. 120 (2004) 4157.
[21] N.M. Reilly, J.U. Reveles, G.E. Johnson, S.N. Khanna, A.W. Castleman Jr., Chem. Phys. Lett. 435 (2007) 295.
[22] N.M. Reilly, J.U. Reveles, G.E. Johnson, S.N. Khanna, A.W. Castleman Jr., J. Phys. Chem. A 111 (2007) 4158.
[23] N.M. Reilly, J.U. Reveles, G.E. Johnson, J.M. del Campo, S.N. Khanna, A.W. Castleman Jr., J. Phys. Chem. C 111 (2007) 19086.
[24] K.S. Molek, C. Anfuso-Cleary, M.A. Duncan, J. Phys. Chem. A 112 (2008) 9238.
[25] P. Li, D.E. Miser, S. Rabiei, R.T. Yadav, M.R. Hajaligol, Appl. Catal. B: Env. 43 (2003) 151.
[26] Y. Xiong, Z. Li, X. Li, B. Hu, Y. Xie, Inorg. Chem. 43 (2004) 6540.
[27] Y. Zheng, Y. Cheng, Y. Wang, F. Bao, L. Zhou, X. Wei, Y. Zhang, Q. Zheng, J. Phys. Chem. B 110 (2006) 3093.
[28] Á. Szegedi, M. Hegedüs, J.L. Margitfalvi, I. Kiricsi, Chem. Commun. (2005) 1441.
[29] J. Jansson, A.E.C. Palmqvist, E. Fridell, M. Skoglundh, L. Qsterlund, P. ThormRhlen, V. Langer, J. Catal. 211 (2002) 387.
[30] Y. Matsuda, E.R. Bernstein, J. Phys. Chem. A 109 (2005) 314.
[31] H.J. Zhai, L.S. Wang, J. Am. Chem. Soc. 129 (2007) 3022.
[32] F. Dong, S. Heinbuch, S.G. He, Y. Xie, J.J. Rocca, E.R. Bernstein, J. Chem. Phys. 125 (2006) 164318.
[33] H.J. Zhai, J. Döbler, J. Sauer, L.S. Wang, J. Am. Chem. Soc. 129 (2007) 13270.
[34] D.E. Bergeron Jr., A.W. Castleman, N.O. Jones, S.N. Khanna, Nano. Lett. 4 (2004) 261.
[35] H.J. Zhai, S. Li, D.A. Dixon, L.S. Wang, J. Am. Chem. Soc. 130 (2008) 5167.

[36] H.J. Zhai, B. Kiran, L.F. Cui, X. Li, D.A. Dixon, L.S. Wang, J. Am. Chem. Soc. 126 (2004) 16134.
[37] H.J. Zhai, X. Huang, L.F. Cui, X. Li, J. Li, L.S. Wang, J. Phys. Chem. A 109 (2005) 6019.
[38] X. Huang, H.J. Zhai, B. Kiran, L.S. Wang, Angew. Chem. Int. Ed. 44 (2005) 7251.
[39] D. Schröder, M. Engeser, M. Brönstrup, C. Daniel, J. Spandl, H. Hartl, Int. J. Mass Spectrom. 228 (2003) 743.
[40] D. Schröder, J. Roithová, Angew. Chem. Int. Ed. 45 (2006) 5705.
[41] N.O. Jones, B.V. Reddy, F. Rasouli, S.N. Khanna, Phys. Rev. B 72 (2005) 165411.
[42] N.O. Jones, B.V. Reddy, F. Rasouli, S.N. Khanna, Phys. Rev. B 73 (2006) 119901(E).
[43] R.B. Freas, B.I. Dunlap, B.A. Waite, J.E. Campana, J. Chem. Phys. 86 (1987) 1276.
[44] M.E. Geusic, M.D. Morse, S.C. O'Brien, R.E. Smalley, Rev. Sci. Instrum. 56 (1985) 2123.
[45] F. Dong, S. Heinbuch, Y. Xie, J.J. Rocca, E.R. Bernstein, Z.-C. Wang, K. Deng, S.-G. He, J. Am. Chem. Soc. 130 (2008) (1932).
[46] A.D. Becke, Phys. Rev. A 38 (1988) 3098.
[47] A.D. Becke, J. Chem. Phys. 98 (1993) 5648.
[48] C. Lee, W. Yang, R.G. Parr, Phys. Rev. B 37 (1988) 785.
[49] P.J. Hay, W.R. Wadt, J. Chem. Phys. 82 (1985) 270.
[50] W.R. Wadt, P.J. Hay, J. Chem. Phys. 82 (1985) 284.
[51] P.J. Hay, W.R. Wadt, J. Chem. Phys. 82 (1985) 299.
[52] T.H. Dunning Jr., P.J. Hay, in: H.F. Schaefer III (Ed.), Modern Theoretical Chemistry, vol.3, Plenum, New York, 1976, pp. 1–28.
[53] M.J. Frisch, G.W. Trucks, H.B. Schlegel, G.E. Scuseria, M.A. Robb, J.R. Cheeseman, J.A. Montgomery Jr., T. Vreven, K.N. Kudin, J.C. Burant, J.M. Millam, S.S. Iyengar, J. Tomasi, V. Barone, B. Mennucci, M. Cossi, G. Scalmani, N. Rega, G.A. Petersson, H. Nakatsuji, M. Hada, M. Ehara, K. Toyota, R. Fukuda, J. Hasegawa, M. Ishida, T. Nakajima, Y. Honda, O. Kitao, H. Nakai, M. Klene, X. Li, J.E. Knox, H.P. Hratchian, J.B. Cross, V. Bakken, C. Adamo, J. Jaramillo, R. Gomperts, R.E. Stratmann, O. Yazyev, A.J. Austin, R. Cammi, C. Pomelli, J. Ochterski, P.Y. Ayala, K. Morokuma, G.A. Voth, P. Salvador, J.J. Dannenberg, V.G. Zakrzewski, S. Dapprich, A.D. Daniels, M.C. Strain, O. Farkas, D.K. Malick, A.D. Rabuck, K. Raghavachari, J.B. Foresman, J.V. Ortiz, Q. Cui, A.G. Baboul, S. Clifford, J. Cioslowski, B.B. Stefanov, G. Liu, A. Liashenko, P. Piskorz, I. Komaromi, R.L. Martin, D.J. Fox, T. Keith, M.A. Al-Laham, C.Y. Peng, A. Nanayakkara, M. Challacombe, P.M.W. Gill, B.G. Johnson, W. Chen, M.W. Wong, C. Gonzalez, J.A. Pople, GAUSSIAN 03 (Revision B.05), Gaussian, Inc., Wallingford, CT, 2004.
[54] http://physics.nist.Gov/PhysRefData/Compositions/index.html.
[55] X.L. Ding, W. Xue, Y.P. Ma, Z.C. Wang, S.G. He, J. Chem. Phys. 130 (2009) 014303.
[56] D. Schröder, A. Fiedler, J. Schwarz, H. Schwarz, Inorg. Chem. 33 (1994) 5094.
[57] W.A. Herrmann, D. Schröder, A. Fiedler, H. Schwarz, Angew. Chem. Int. Ed. 34 (1995) 2517.
[58] A. Fiedler, I. Kretzschmar, D. Schröder, H. Schwarz, J. Am. Chem. Soc. 118 (1996) 9941.
[59] K.R. Asmis, M. Brümmer, C. Kaposta, G. Santambrogio, G. von Helden, G. Meijer, K. Rademannd, L. Wöste, Phys. Chem. Chem. Phys. 4 (2002) 1101.
[60] S. Feyel, D. Schröder, H. Schwarz, Eur. J. Inorg. Chem. (2008) 4961.
[61] O. Gehret, M.P. Irion, Chem. Eur. J. 2 (1996) 598.
[62] P. Jacksona, J.N. Harvey, D. Schröder, H. Schwarz, Int. J. Mass Spectrom. 204 (2001) 233.
[63] S.F. Vyboishchikov, J. Sauer, J. Phys. Chem. A 105 (2001) 8588.
[64] M.N. Yi, K.J. Fisher, I.G. Dance, Int. J. Mass. Spectrum. 216 (2002) 155.
[65] J.F. Huang, A.N. Hung, C.B. Wang, C.T. Yeh, J. Chin. Chem. Soc. 49 (2002) 819.
[66] B.V. Reddy, S.N. Khanna, Phys. Rev. B 54 (1996) 2240.
[67] B. Wang, S. Nagase, J. Zhao, G. Wang, J. Phys. Chem. C 111 (2007) 4956.